

### Electromagnetic transitions in <sup>14</sup>C and <sup>14</sup>N

R. L. Kozub, J. Lin, and J. F. Mateja

Department of Physics, Tennessee Technological University, Cookeville, Tennessee 38501

C. J. Lister, D. J. Millener, and E. K. Warburton

Brookhaven National Laboratory, Upton, New York 11973

(Received 11 September 1980)

The lifetimes of the  $J^\pi = 0^+$  6590-keV and  $J^\pi = 3^-$  6728-keV states in <sup>14</sup>C and the  $J^\pi = 3^-$  5834-keV state in <sup>14</sup>N were measured using the recoil distance method. Gamma rays following the  $pn$  and  $2n$  evaporation channels from <sup>9</sup>Be + <sup>7</sup>Li reactions were detected at  $\theta_\gamma = 0^\circ$ . The experimental results are <sup>14</sup>C(6590,0<sup>+</sup>),  $\tau = 3.7 \pm 0.9$  ps; <sup>14</sup>C(6728,3<sup>-</sup>),  $\tau = 96 \pm 15$  ps; <sup>14</sup>N(5834,3<sup>-</sup>),  $\tau = 12.9 \pm 1.9$  ps. Extensive shell-model calculations for both <sup>14</sup>C and <sup>14</sup>N have been performed using an SU(3) basis and are compared to these and other experimental results.

NUCLEAR REACTIONS <sup>7</sup>Li(<sup>9</sup>Be,  $pn\gamma$ )  $E_{Be} = 5.5$  MeV; <sup>9</sup>Be(<sup>7</sup>Li,  $pn\gamma$ ) and <sup>9</sup>Be(<sup>7</sup>Li,  $2n\gamma$ )  $E_{Li} = 3.8$ – $7.8$  MeV; measured  $E_\gamma, I_\gamma$  (recoil distance method); calculated  $\tau$  from theory and compared with experiment.

#### I. INTRODUCTION

One of the early successes of the extended shell model was the prediction<sup>1</sup> and identification<sup>2,3</sup> of 0, 1, and 2  $\hbar\omega$  configurations among the bound levels of <sup>14</sup>C–<sup>14</sup>N. The investigations of the electromagnetic transitions connecting these levels provided the major experimental evidence for the configurational assignments, as well as systematics of great use in later  $\gamma$ -ray studies of the energy levels of light nuclei.

In view of the early extensive effort in the  $\gamma$ -ray spectroscopy of mass 14 it is very surprising that some 20 years later the lifetimes of the first two excited states of <sup>14</sup>C were still unknown.<sup>4,5</sup> The aim of the present study was to measure the lifetime of the second-excited state at 6590 keV and thus provide a further test of multiconfigurational shell-model calculations. The state has  $J^\pi = 0^+$  and decays predominantly by an  $E1$  transition to the  $J^\pi = 1^-$  6094-keV level, with a weak (1.0  $\pm$  0.4%)  $E0$  branch to the ground state.<sup>7</sup>

Lower limits of >1.2 and 0.6 ps have been set for its mean life<sup>5,7</sup> and thus it was expected that the lifetime would be in the region accessible to the Doppler shift recoil distance method (RDM).<sup>8,9</sup>

The present work describes the measurement of the lifetime of the 6590-keV state in <sup>14</sup>C using the RDM and the <sup>7</sup>Li(<sup>9</sup>Be,  $pn\gamma$ )<sup>14</sup>C reaction. In addition, lifetimes were measured for the  $J^\pi = 3^-$  6728-keV level of <sup>14</sup>C and the  $J^\pi = 3^-$  5834-keV level of <sup>14</sup>N (Fig. 1) using the inverted (<sup>7</sup>Li,  $pn\gamma$ ) and (<sup>7</sup>Li,  $2n\gamma$ ) reactions on <sup>9</sup>Be. Finally, shell-model calculations for selected mass 14 transitions were performed using an SU(3) basis. A feature of this model is the symmetry of the basis states, which permits an exact elimination of the spurious cen-

ter-of-mass states which usually plague calculations of  $E1$  and  $M2$  transitions.

#### II. EXPERIMENTAL METHOD AND RESULTS

An excitation function for the <sup>9</sup>Be + <sup>7</sup>Li system was measured using a 200- $\mu$ g/cm<sup>2</sup> Be target at <sup>7</sup>Li energies between 3.8 and 7.8 MeV. Yield curves taken at  $\theta_\gamma = 90^\circ$  for the 495-keV (6590–6094) transition in <sup>14</sup>C and the 728-keV (5834–5107) transition in <sup>14</sup>N are shown in Fig. 2. The

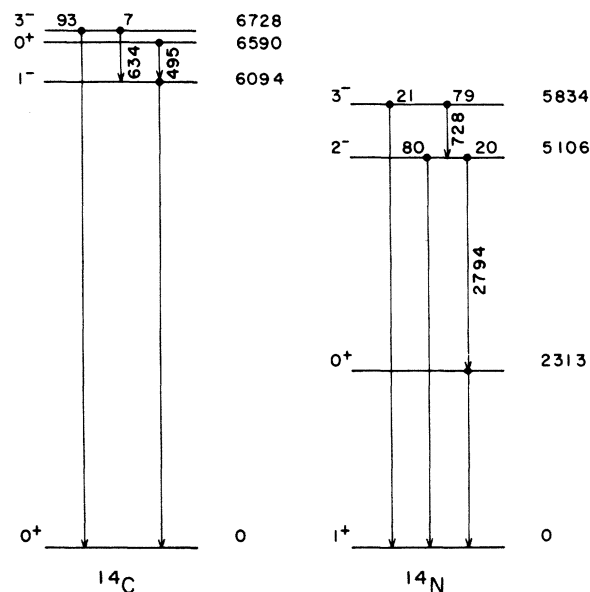


FIG. 1. Decay schemes for low-lying levels in <sup>14</sup>C and <sup>14</sup>N, showing transitions pertinent to the present experimental work. The excitation energies (in keV) and branching ratios (in percent) are from Ref. 4 and the text.

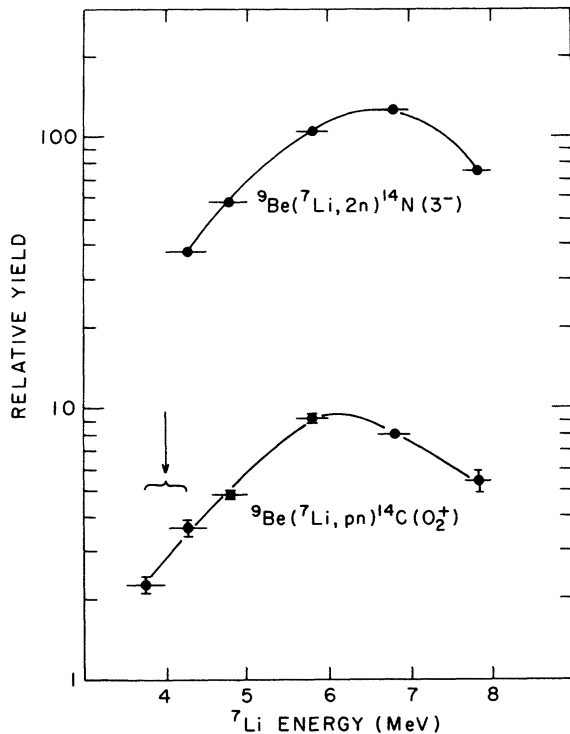


FIG. 2. Yield of  $\gamma$  rays from the 5834  $\rightarrow$  5106 transition in  $^{14}\text{N}$  and the 6590  $\rightarrow$  6094 transition in  $^{14}\text{C}$  as a function of  $^7\text{Li}$  bombarding energy. Vertical error bars are statistical, while horizontal bars reflect the range of  $^7\text{Li}$  energies in the  $^9\text{Be}$  target for each data point. The energy range used for the Li-target RDM measurement is indicated by the arrow.

$^{14}\text{C}$  495-keV  $\gamma$  ray was easily visible in the  $90^\circ$  spectra, but at  $0^\circ$  it was obscured by the flight peak from the 478-keV  $1-0$  transition in  $^7\text{Li}$ . A similar problem was encountered in the RDM measurement (using the Li target) at energies near the peak in the excitation curve. The RDM measurement was thus performed at a lower energy, indicated by the arrow in Fig. 2, where the peak-to-background ratio was more favorable.

A schematic diagram of the target and detector geometry in and near the RDM apparatus is shown in Fig. 3. A 30-nA beam of  $^9\text{Be}^+$  ions was accelerated to 10 MeV by the BNL Tandem MP-6 and was then degraded by a 5-mg/cm $^2$  Ta backing such that the energy upon entering the 150- $\mu\text{g}/\text{cm}^2$  Li target was approximately 5.5 MeV. Recoils were stopped by a gold stopper which could be positioned electrically to an accuracy of  $\pm 1$   $\mu\text{m}$ . Electrical contact between target and stopper was made at  $d = 7$   $\mu\text{m}$ , and our closest data point was at 11  $\mu\text{m}$ . The capacitance of the target-stopper system was measured as a function of stopper distance  $d$  and these data were used to extract the zero distance point to an accuracy of  $\pm 2$   $\mu\text{m}$  by fitting a curve calcu-

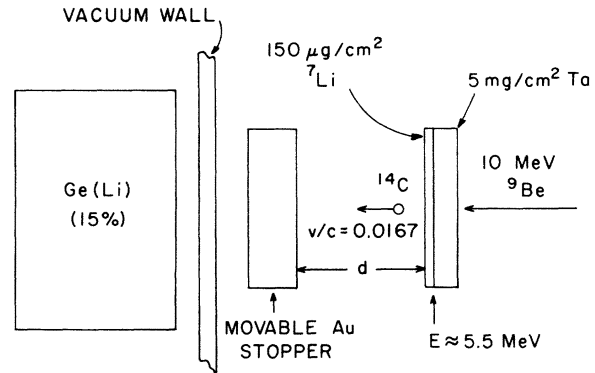


FIG. 3. Schematic arrangement of target, stopper, and detector for the RDM measurement with the Li target (not to scale).

lated from the actual shapes of the two conductors.

The recoil velocity used for lifetime measurements following  $pn$  and  $2n$  evaporation was determined from the centroids of the stopped and moving components of the 2313-keV  $1-0$  transition in  $^{14}\text{N}$ . Including a 3% correction due to the finite solid angle subtended by the Ge(Li) detector our measured result is  $v/c = 0.0167 \pm 0.0002$ . This value is consistent with that expected for  $A = 14$  recoils from a fusion-evaporation reaction. The total intensity (shifted plus unshifted) of the 2313-keV transition was used to normalize the yield of the stopped component of the 495-keV transition at each flight distance. A zero distance point was taken by removing the Li from the Ta support foil and evaporating 40  $\mu\text{g}/\text{cm}^2$  of Li onto a Ta stopper. This point could be normalized to the other data, despite the difference in target thickness, as the yield curves of 2313-keV and 495-keV transitions are very similar at Be energies near 5.1 MeV (Fig. 2).

Portions of two spectra taken as part of the RDM measurement are shown in Fig. 4. Sharp contaminant lines appear just above and below the stopped component of the 495-keV transition. They have energies of  $492.2 \pm 0.3$  and  $499.8 \pm 0.2$  keV. In extensive surveys of  $\gamma$ -ray spectra from light ion bombardment of  $^7\text{Li}$  we observed only two  $\gamma$  rays other than the 495-keV line in the energy region 480–510 keV. These had energies of  $493 \pm 1$  and  $500 \pm 1$  keV, were observed in  $^7\text{Li} + ^{16}\text{O}$ , and were assigned to  $^{23}\text{Ne}(2315-1823)$  and to  $^{24}\text{Na}(1885-1347)$  and/or  $^{17}\text{N}(3629-3129)$ . The 492- and 500-keV lines observed in the present study can probably be associated with these transitions following  $^9\text{Be}$  reactions on  $^{16}\text{O}$  and  $^{12}\text{C}$  contaminants in the target. The 495-keV transition can contain a contribution from the  $^{17}\text{F}$  495- $0$  transition. If so, it would contribute to the long-lived background (discussed below) since the  $^{17}\text{F}$  495-keV level has

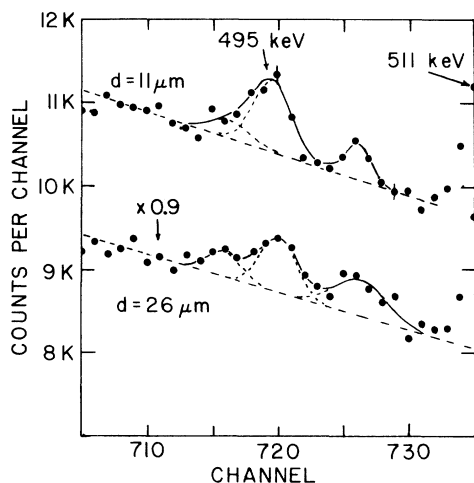


FIG. 4. Portions of  $\gamma$ -ray spectra ( $\theta_\gamma = 0^\circ$ ) taken with  $d = 11$  and  $26 \mu\text{m}$  as part of the RDM measurement of the mean life of the 6590-keV level of  $^{14}\text{C}$  via the  $^7\text{Li}(^9\text{Be}, pn)\gamma^{14}\text{C}$  reaction. The peak-fitting procedure is described in the text. The two unidentified  $\gamma$ -ray peaks are discussed in the text.

a mean life of 412 ps.<sup>4</sup>

The yields were extracted using an exponential background and three Gaussian shapes. The decay curve for the 495-keV transition is shown in Fig. 5. The data were fitted using an exponential decay plus a constant background. Relativistic and finite solid angle corrections were included following the methods outlined by Jones *et al.*<sup>10</sup> The background evident in Fig. 5 is attributed to some of the recoils stopping in the target due to nonuniformities

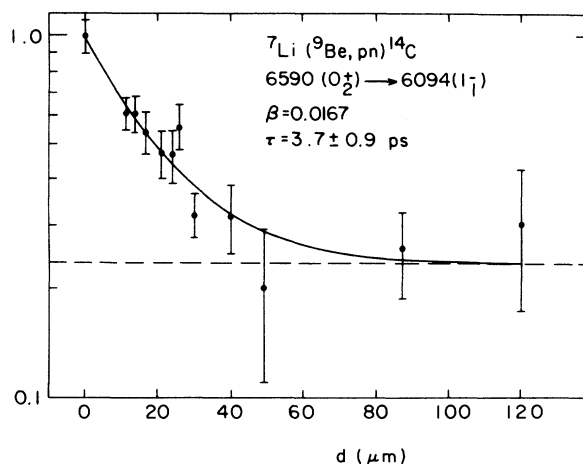


FIG. 5. Decay curve for the 495-keV transition in  $^{14}\text{C}$ . The fitting procedure is described in the text.

(which may be the result of partial oxidation of the target) and to large angle scattering.

Our final value for the mean life is

$$\tau = 3.7 \pm 0.9 \text{ ps},$$

where the uncertainty includes all the known sources of systematics and statistical error. This result supercedes the preliminary value for  $\tau$  given in Ref. 11, and is in agreement with a recent measurement using the  $^2\text{H}(^{13}\text{C}, p)^{14}\text{C}$  reaction ( $\tau = 4.6 \pm 0.7 \text{ ps}$ ).<sup>12</sup>

A separate RDM experiment was performed using a  $200\text{-}\mu\text{g}/\text{cm}^2$   $^9\text{Be}$  target and a 6.5-MeV  $^7\text{Li}$  beam, which resulted in a recoil velocity of  $v/c$

TABLE I. Summary of experimental results for the levels whose lifetimes were measured in the present investigation.

Nucleus	$E_i(J_i^\pi)$ (keV)	$E_f(J_f^\pi)$ (keV)	$E_T$ (keV)	Branching ratio %	Mean lifetime $\tau$ (ps)		
					Present	Previous	Weighted Mean
$^{14}\text{C}$	6728( $3^-$ )	0( $0^+$ )	6728	93 $\pm 2^a$	96 $\pm 15$	97 $\pm 15^b$	96 $\pm 11$
		6094( $1^-$ )	634	7 $\pm 2^a$			
$^{14}\text{C}$	6590( $0^+$ )	0( $0^+$ )	6590	1.1 $\pm 0.1^f$	3.7 $\pm 0.9$	>0.6 <sup>a</sup>	4.2 $\pm 0.6$
		6094( $1^-$ )	495	98.9 $\pm 0.1^f$		>1.2 <sup>c</sup> 4.6 $\pm 0.7^f$	
$^{14}\text{N}$	5834( $3^-$ )	0( $1^+$ )	5834	21.3 $\pm 1.3^d$	12.9 $\pm 1.9$	13.7 $\pm 1.1^e$	13.2 $\pm 0.7$
		5106( $2^-$ )	728	78.7 $\pm 1.3^d$		12.8 $\pm 1.0^f$ 18 $\pm 2^g$	

<sup>a</sup> Reference 7 and present results (see text).

<sup>b</sup> Reference 13.

<sup>c</sup> Reference 5.

<sup>d</sup> The adopted value from the 1970 compilation [F. Ajzenberg-Selove, Nucl. Phys. A152, 1 (1970)]. These weighted mean values include some measurements of Young, Phillips, and Marion. From the first-hand experience of one of us (E.K.W.) these measurements were of unusually high reliability, and so we retain them even though they have not been published.

<sup>e</sup> Reference 14.

<sup>f</sup> Reference 12.

<sup>g</sup> Reference 15.

= 0.0163 ± 0.0002. Data were taken over the distance range 36–3845 μm. As expected, the background encountered at large distances (i.e., the presence of stopped components in the line shapes) was greatly reduced in these data thus supporting the contention that the background evident in Fig. 5 is largely due to oxidation of the <sup>7</sup>Li target. As mentioned earlier, the Doppler broadened and shifted <sup>7</sup>Li 478-keV transition was quite intense and obscured the <sup>14</sup>C 495-keV transition. Thus, these data yielded no additional information on the <sup>14</sup>C 6590-keV level but lifetimes were extracted for the <sup>14</sup>C 6728- and <sup>14</sup>N 5834-keV levels utilizing the <sup>14</sup>C 6728–0 and <sup>14</sup>N 728-keV 5834–5106 transitions.

The results of all three mean life determinations are given in Table I together with previous measurements.<sup>4, 5, 7, 12–15</sup> A discrepancy<sup>4, 7, 16</sup> over the branching ratios of the <sup>14</sup>C  $J^\pi = 3^-$  6728-keV level was resolved by the present data, the branching ratios deduced were 93 ± 2% and 7 ± 2% for the 6728–0 and 6728–6094 transitions, respectively, in agreement with Alburger *et al.*<sup>7</sup>

Energy determinations were made of the <sup>14</sup>C 6590–6094 and <sup>14</sup>N 5834–5106 γ transitions during the excitation function measurements. The results are 495.35 ± 0.10 and 728.34 ± 0.10 keV, respectively. The latter result, corrected for nuclear recoil, and added to the excitation energy of the state at 5105.87 ± 0.18 keV (Ref. 4) yields 5834.23 ± 0.21 keV for the sixth-excited state of <sup>14</sup>N.

The data collected in Table II for the decay of additional levels in <sup>14</sup>C and <sup>14</sup>N are pertinent to the shell-model calculations presented in the next section. These data are all from previous experiments<sup>4, 5, 14–18</sup> and are given here because, for one reason or another, their extraction from the literature is not straightforward.

For both the <sup>14</sup>N 5106- and 5834-keV levels the measurements<sup>15</sup> of Allen *et al.* are in poor agreement (see Tables I and II) with the other measurements. For the 5834-keV level our data (see Table I) favors the more recent results.<sup>12, 14</sup> Thus we adopt the result of Moorhouse *et al.*<sup>14</sup> for the 5106-keV level and exclude the result of Allen *et al.* in obtaining the weighted mean for the 5834-keV level.

### III. SHELL MODEL CALCULATIONS

#### A. Introduction

The most extensive shell-model calculation to date for the  $A = 14$  system is the weak coupling calculation of Lie<sup>19</sup> which provides an excellent description of levels below 13 MeV in <sup>14</sup>N and the  $T = 1$  analogs in <sup>14</sup>C. Unfortunately, the  $E1$  matrix element corresponding to the dominant decay mode

of the 6.59-MeV,  $J^\pi, T = 0_2^+, 1$  level in <sup>14</sup>C cannot be calculated within the framework of Lie's model. Also Lie did not calculate any  $M2$  matrix elements. The present shell-model calculation is performed in an  $SU(3)$  basis. Spurious center of mass (c.m.) states are removed from the basis, thus eliminating a major source of error in the calculation of  $E1$  and  $M2$  matrix elements. Of course, these matrix elements are still difficult to calculate since they are generally very much hindered with respect to single-particle estimates.

The lowest negative-parity levels of  $A = 14$  are expected to be well described in a  $1\bar{n}\omega$  basis (Lie obtains very small  $3\bar{n}\omega$  admixtures) and to have a simple weak-coupling structure, predominantly a  $0d_{5/2}$  or  $1s_{1/2}$  nucleon coupled to the  $J^\pi, T = \frac{1}{2}^-, \frac{1}{2}$  or  $\frac{3}{2}^-, \frac{1}{2}$  states of the  $A = 13$  core. Our calculation is, with some minor modifications, the same as that of Millener and Kurath.<sup>20</sup>

For the positive parity levels it is important to consider at least  $0\bar{n}\omega$  and  $2\bar{n}\omega$  excitations. Indeed, the 6590-keV  $0_2^+, 1$  level of <sup>14</sup>C is thought to have a dominantly 2p-4h structure consistent with the main  $^{12}\text{C}(0_1^+, 0) \otimes ^{18}\text{O}(0_1^+, 1)$  component in Lie's wave function. We include in our basis those  $s^4p^8(sd)^2$ ,  $s^4p^9(pf)$ , and  $s^3p^{10}(sd)$  configurations with  $(\lambda\mu) = (44), (06), (14), (25), (52), (60), (32),$  and  $(41)$  leaving out all configurations with  $(\lambda\mu) = (30), (03), (11),$  and  $(00)$ . The omitted configurations would make a very small contribution to the  $0_1^+, 1$  wave function but could make non-negligible contributions to the  $E1$  matrix element. Thus the adequacy of the truncation should be investigated carefully. For the  $p$ -shell interaction we use the (8-16)2BME interaction of Cohen and Kurath,<sup>21</sup> for the  $sd$  shell that of Chung and Wildenthal,<sup>22</sup> for the  $ph$  interaction a modification of the MK interaction of Millener and Kurath,<sup>20</sup> and for all other matrix elements we compute from the modified MK potential.

The single-particle energies for the  $0p$  orbits are fixed at the Cohen and Kurath values<sup>21</sup> which reproduce the "single hole" splitting in  $A = 15$ . The single-particle energies for the  $sd$  shell are chosen<sup>20</sup> to reproduce the binding energies of the "single-particle" levels of <sup>17</sup>O once the contribution to the single-particle energies from the MK interaction has been taken into account.

#### B. Results

Electromagnetic matrix elements are calculated for transitions between the lowest negative-parity levels of <sup>14</sup>N and <sup>14</sup>C and for transitions between these negative-parity levels and the lowest  $0^+$  and  $1^+$  levels. The results are given in Table III. For transitions involving the positive-parity levels, matrix

TABLE II. Experimental results for some additional mass 14  $\gamma$  decays.

Nucleus	$E_i(J_i^\pi)$ (MeV)	$E_f(J_f^\pi)$ (MeV)	$E_T$ (MeV)	Branching ratio (%)	$\tau$ or $\Gamma_\gamma$ (ps) or (eV)	Mixing ratio	References <sup>a</sup>	
$^{14}\text{C}$	7.34( $2^-$ )	0( $0^+$ )	7.34	16 $\pm$ 3	0.16 $\pm$ 0.06 ps	$E2/M1: -0.04 \pm 0.09$ $E2/M1: +0.07 \pm 0.03$	b;c	
		6.09( $1^-$ )	1.25	50 $\pm$ 3			b;c;d	
		6.73( $3^-$ )	0.61	34 $\pm$ 3			b;c;d	
$^{14}\text{N}$	5.11( $2^-$ )	0( $1^+$ )	5.11	79.9 $\pm$ 1.0	6.2 $\pm$ 0.4 ps	$M2/E1: -0.16 \pm 0.02$ $E3/E1: -0.15 \pm 0.025$	e; f, g; h	
		2.31( $0^+$ )	2.79	19.4 $\pm$ 1.2	12.4 $\pm$ 1.4 ps		e	
		3.95( $1^+$ )	1.16	0.7 $\pm$ 0.4	unknown		e	
	8.06( $1^-$ )	0( $1^+$ )	8.06	80.3 $\pm$ 0.6	9.9 $\pm$ 2.5 eV	0	0 (assumed) unknown	
		2.31( $0^+$ )	5.75	1.40 $\pm$ 0.14	0.17 $\pm$ 0.05 eV			
		3.95( $1^+$ )	4.11	12.7 $\pm$ 0.4	1.56 $\pm$ 0.40 eV			
		4.92( $0^-$ )	3.14	1.86 $\pm$ 0.14	0.23 $\pm$ 0.06 eV			
		5.11( $2^-$ )	2.95	0.25 $\pm$ 0.14	0.03 $\pm$ 0.02 eV			
		5.69( $1^-$ )	2.37	3.5 $\pm$ 0.4	0.43 $\pm$ 0.12 eV			
		$\Gamma_\gamma$ (total) = 12.3 $\pm$ 3.1 eV						j; k, l
	$^{14}\text{N}$	8.49( $4^-$ )	5.11( $2^-$ )	3.38	83 $\pm$ 3	0.088 $\pm$ 0.020 ps	0 (assumed) unknown	i; i
5.83( $3^-$ )			2.66	17 $\pm$ 3		i		
8.79( $0^-$ )		0( $1^+$ )	8.79	90 $\pm$ 10	46 $\pm$ 12 eV	0	0 (assumed) unknown	
		$\Gamma_\gamma$ (total) = 51 $\pm$ 13 eV						m; l
8.91( $3^-$ )		0	8.91	1.6 $\pm$ 0.5	0.0066 $\pm$ 0.0022 eV	0	0 (assumed) unknown	n; n
		5.11	3.80	5.4 $\pm$ 2.5	0.023 $\pm$ 0.012 eV			o
		5.83	3.08	89 $\pm$ 3	0.37 $\pm$ 0.10 eV			o
		6.44	2.47	3 $\pm$ 1	0.012 $\pm$ 0.005 eV			o
		7.03	1.88	1.4 $\pm$ 0.8	0.006 $\pm$ 0.004 eV			o
$\Gamma_\gamma$ (total) = 0.42 $\pm$ 0.12 eV						o, n; m		
9.51( $2^-$ )	0( $1^+$ )	9.51	<0.16	<0.008 eV	0	0 (assumed) unknown		
	3.95( $1^+$ )	5.56	6 $\pm$ 1	0.30 $\pm$ 0.09 eV				
	5.11( $2^-$ )	4.40	78 $\pm$ 3	3.84 $\pm$ 0.97 eV				
	5.83( $3^-$ )	3.68	16 $\pm$ 2	0.79 $\pm$ 0.22 eV				
$\Gamma_\gamma$ (total) = 4.9 $\pm$ 1.2 eV						o; m		

<sup>a</sup> References for the branching ratios; mean lives or radiative widths; mixing ratios.

<sup>b</sup> Average of the two measurements quoted in Ref. 4.

<sup>c</sup> Reference 5.

<sup>d</sup> Reference 16.

<sup>e</sup> Reference 4. Note these weighted average include the results of Young, Phillips, and Marion (see footnote d, Table I).

<sup>f</sup> Reference 14.

<sup>g</sup> Reference 15.

<sup>h</sup> These are the weighted averages of the values obtained by Blake *et al.* (Ref. 17) and Gorodetzky *et al.* (Ref. 17) after changing to the sign convention of Ref. 18.

<sup>i</sup> J. Keinonen, A. Anttila, and M Bister, Nucl. Phys. **A294**, 1 (1978).

<sup>j</sup> M. J. Renan, J. P. F. Sellschop, R. J. Keddy, and D. W. Mingay, Nucl. Phys. **A193**, 470 (1972).

<sup>k</sup> D. F. Hebbard and J. L. Vogl, Nucl. Phys. **21**, 652 (1961).

<sup>l</sup> J. D. Seagrave, Phys. Rev. **85**, 197 (1952).

<sup>m</sup> H. H. Woodbury, R. B. Day, and A. V. Tollestrup, Phys. Rev. **92**, 1199 (1953).

<sup>n</sup> H.-G. Clerc and E. Kuphal, Z. Phys. **211**, 452 (1968).

<sup>o</sup> Reference 2.

elements are given for the two cases of no-mixing and mixing of the  $0\hbar\omega$  and  $2\hbar\omega$  configurations. A breakdown of the wave functions for the no-mixing case in terms of the intensity of each SU(3) representation is given in Table IV. This is a rather

coarse characterization of the wave functions but it illustrates the configurational similarities of the lowest  $2\hbar\omega$  and  $1\hbar\omega$  levels. Table IV is also useful in a discussion of E1 selection rules.

If harmonic oscillator wave functions are used

TABLE III. Comparison of shell-model predictions to experiment for electromagnetic transitions in  $^{14}\text{C}$  and  $^{14}\text{N}$ .

$E_i - E_f$ (MeV)	$J_i^\pi T_i \rightarrow J_f^\pi T_f$	Quantity <sup>a</sup>	Theory <sup>b</sup>	Experiment <sup>c</sup>
$^{14}\text{C}$				
6.09 → 0	$1_1^-, 1 \rightarrow 0_1^+, 1$	$B(E1)$	$2.05 \times 10^{-2}$ ( $2.14 \times 10^{-2}$ )	
6.59 → 6.09	$0_2^+, 1 \rightarrow 1_1^-, 1$	$B(E1)$	$3.26 \times 10^{-3}$ ( $5.33 \times 10^{-4}$ )	$(3.3 \pm 0.5) \times 10^{-3}$
6.73 → 0	$3_1^-, 1 \rightarrow 0_1^+, 1$	$B(E3)$	0.39 (0.58)	$2.33 \pm 0.27$
6.73 → 6.09	$3_1^-, 1 \rightarrow 1_1^-, 1$	$B(E2)$	1.88	$2.90 \pm 0.87$
6.90 → 6.09	$0_1^-, 1 \rightarrow 1_1^-, 1$	$B(M1)$	0.89	$1.67 \pm 0.17$
7.34 → 0	$2_1^-, 1 \rightarrow 0_1^+, 1$	$B(M2)$	0.34 (0.24)	$0.37 \pm 0.16$
7.34 → 6.09	$2_1^-, 1 \rightarrow 1_1^-, 1$	$B(M1)$	$6.15 \times 10^{-3}$	$(5.1 \pm 1.9) \times 10^{-2}$
		$B(E2)$	0.70	
		$\chi(E2/M1)$	-0.12	$-(0.04 \pm 0.09)$
		$\tau$ (fs)	2633	$340 \pm 130$
7.34 → 6.73	$2_1^-, 1 \rightarrow 3_1^-, 1$	$B(M1)$	$9.5 \times 10^{-2}$	$0.29 \pm 0.11$
		$B(E2)$	5.61	
		$\chi(E2/M1)$	-0.04	$+0.07 \pm 0.30$
		$\tau$ (fs)	1453	$460 \pm 180$
$^{14}\text{N}$				
5.11 → 0	$2_1^-, 0 \rightarrow 1_1^+, 0$	$B(E1)$		$(1.70 \pm 0.12) \times 10^{-6}$
		$B(M2)$	$1.02 \times 10^{-5}$ ( $1.54 \times 10^{-2}$ )	$(7.0 \pm 1.9) \times 10^{-3}$
		$B(E3)$	3.49 (3.51)	$4.6 \pm 1.5; 4.1 \pm 1.0^d$
		$\chi(E3/M2)$	+43 (+1.1)	$+0.94 \pm 0.20^e$
5.11 → 2.31	$2_1^-, 0 \rightarrow 0_1^+, 1$	$B(M2)$	2.15 (1.79)	$1.42 \pm 0.13$
5.11 → 3.95	$2_1^-, 0 \rightarrow 1_2^+, 0$	$B(E1)$		$(1.2 \pm 0.7) \times 10^{-5}$
		$B(M2)$	$8.79 \times 10^{-2}$ ( $9.12 \times 10^{-2}$ )	
		$\chi(M2/E1)$	0.15 (0.15) <sup>f</sup>	
5.69 → 2.31	$1_1^-, 0 \rightarrow 0_1^+, 1$	$B(E1)$	$8.76 \times 10^{-3}$ ( $5.07 \times 10^{-3}$ )	$(2.6 \pm 0.5) \times 10^{-2}$
5.83 → 0	$3_1^-, 0 \rightarrow 1_1^+, 0$	$B(M2)$	$1.17 \times 10^{-2}$ ( $1.4 \times 10^{-2}$ )	$(7.6 \pm 2.2) \times 10^{-3}$
		$B(E3)$	2.96 (3.54)	$6.2 \pm 1.9; 6.1 \pm 1.3^d$
		$\chi(E3/M2)$	-1.33 (-1.33)	$-1.20 \pm 0.30^e$
		$\tau$ (ps)	35.4 (29.5)	$62.0 \pm 5.9$
5.83 → 5.11	$3_1^-, 0 \rightarrow 2_1^-, 0$	$B(M1)$	$7.27 \times 10^{-3}$	$(4.94 \pm 0.34) \times 10^{-3}$
		$B(E2)$	$4.78 \times 10^{-2}$	
		$\chi(E2/M1)$	-0.02	$-0.05 \pm 0.04^h$
		$\tau$ (ps)	11.4	$16.8 \pm 1.3$
8.06 → 0	$1_2^-, 1 \rightarrow 1_1^+, 0$	$B(E1)$	$2.36 \times 10^{-2}$ ( $9.53 \times 10^{-3}$ )	$(3.9 \pm 1.0) \times 10^{-2}$
		$\Gamma_\gamma$ (eV)	4.84 (1.96)	$9.9 \pm 2.5$
8.06 → 3.95	$1_2^-, 1 \rightarrow 1_2^+, 0$	$B(E1)$	$1.03 \times 10^{-2}$ ( $1.81 \times 10^{-2}$ )	$(7.0 \pm 1.8) \times 10^{-2}$
		$\Gamma_\gamma$ (eV)	0.28 (0.50)	$1.6 \pm 0.4$
8.06 → 4.92	$1_2^-, 1 \rightarrow 0_1^-, 0$	$B(M1)$	0.40	$0.36 \pm 0.10$
8.06 → 5.69	$1_2^-, 1 \rightarrow 1_1^-, 0$	$B(M1)$	1.46	$1.55 \pm 0.43$
		$\Gamma_\gamma$ (eV)	0.40	$0.43 \pm 0.12$
8.49 → 5.11	$4_1^-, 0 \rightarrow 2_1^-, 0$	$B(E2)$	4.5	$8.7 \pm 2.2^h$
8.49 → 5.83	$4_1^-, 0 \rightarrow 3_1^-, 0$	$B(M1)$	$1.35 \times 10^{-3}$	$(3.3 \pm 1.0) \times 10^{-31, j}$
		$B(E2)$	5.6	$8.3 \pm 2.9^{i, j}$
		$\chi(E2/M1)$	+1.51	
		$\tau$ (fs)	385	$520 \pm 130$
8.79 → 0	$0_2^-, 1 \rightarrow 1_1^+, 0$	$B(E1)$	0.11 (0.18)	$0.18 \pm 0.05$
8.79 → 3.95	$0_2^-, 1 \rightarrow 1_2^+, 0$	$B(E1)$	$8.89 \times 10^{-3}$ ( $1.25 \times 10^{-3}$ )	

TABLE III. (Continued)

$E_i \rightarrow E_f$ (MeV)	$J_i^\pi T_i \rightarrow J_f^\pi T_f$	Quantity <sup>a</sup>	Theory <sup>b</sup>	Experiment <sup>c</sup>
8.91 $\rightarrow$ 0	$3_2^-, 1 \rightarrow 1_1^+, 0$	$B(M2)$	2.47 (1.97)	1.38 $\pm$ 0.45
		$B(E3)$	0.45 (0.20)	
		$x(E3/M2)$	-0.027 (-0.020)	
		$\Gamma_\gamma$ (eV)	$1.2 \times 10^{-2}$ ( $9.5 \times 10^{-3}$ )	(6.6 $\pm$ 2.2) $\times 10^{-3}$
8.91 $\rightarrow$ 5.11	$3_2^-, 1 \rightarrow 2_1^-, 0$	$B(M1)$	$4.51 \times 10^{-3}$	(1.8 $\pm$ 1.0) $\times 10^{-2}$
		$B(E2)$	0.136	
		$x(E2/M1)$	-0.18	
		$\Gamma_\gamma$ (eV)	$5.31 \times 10^{-3}$	(2.3 $\pm$ 1.2) $\times 10^{-2}$
8.91 $\rightarrow$ 5.83	$3_2^-, 1 \rightarrow 3_1^-, 0$	$B(M1)$	0.33	0.61 $\pm$ 0.15 <sup>d</sup>
		$B(E2)$	0.47	
		$x(E2/M1)$	+0.033	
		$\Gamma_\gamma$ (eV)	0.20	0.37 $\pm$ 0.09
9.51 $\rightarrow$ 0	$2_5^-, 1 \rightarrow 1_1^+, 0$	$B(E1)$	$2.77 \times 10^{-4}$ ( $3.32 \times 10^{-4}$ )	$< 2.1 \times 10^{-5}$
		$B(M2)$	0.635 (0.378)	
		$x(M2/E1)$	-0.21 (+0.15)	
		$\Gamma_\gamma$ (eV)	0.09 (0.11)	$< 8 \times 10^{-3}$
9.51 $\rightarrow$ 3.95	$2_5^-, 1 \rightarrow 1_2^+, 0$	$B(E1)$	$3.05 \times 10^{-3}$ ( $2.17 \times 10^{-3}$ )	(4.7 $\pm$ 1.4) $\times 10^{-3}$ <sup>d</sup>
		$\Gamma_\gamma$ (eV)	0.21 (0.15)	0.30 $\pm$ 0.09
9.51 $\rightarrow$ 5.11	$2_5^-, 1 \rightarrow 2_1^-, 0$	$B(M1)$	1.74	2.1 $\pm$ 0.5 <sup>d</sup>
		$\Gamma_\gamma$ (eV)	3.07	3.8 $\pm$ 1.0
9.51 $\rightarrow$ 5.83	$2_5^-, 1 \rightarrow 3_1^-, 0$	$B(M1)$	0.98	0.94 $\pm$ 0.26 <sup>d</sup>
		$\Gamma_\gamma$ (eV)	1.01	0.8 $\pm$ 0.2

<sup>a</sup> The transition strengths  $B(EL)$  and  $B(ML)$  are in Weisskopf units (Ref. 23), the mixing ratios  $x(L+1/L)$  are dimensionless, and the units for the mean lifetimes  $\tau$  are given.

<sup>b</sup> Bare  $g$  factors are used for all magnetic transitions. For  $E2$  transitions the isoscalar effective charge is double the bare value. No effective charge is used for  $E1$  or  $E3$  transitions. The radial matrix elements are computed using oscillator wave functions with  $b=1.699$  fm.

<sup>c</sup> Unless otherwise noted, these results are from data collected in Tables I and II, or from the compilation of Ref. 4. For the decay of the levels above 8-MeV excitation, except the 8.49-MeV level, the transitions are assumed to proceed via the lowest allowed multipolarity.

<sup>d</sup> The ( $e, e'$ ) result of Ref. 24.

<sup>e</sup> From the ratio of the  $x(E3/E1)$  and  $x(M2/E1)$  values of Table II.

<sup>f</sup> The magnitude of the  $M2/E1$  mixing ratio is estimated by using the experimental  $B(E1)$  and the calculated  $B(M2)$ .

<sup>g</sup> Reference 25.

<sup>h</sup> Reference 2.

<sup>i</sup> Reference 26.

<sup>j</sup> The mixing ratio is unknown, hence an upper limit.

to compute the single-particle matrix elements, the  $E1$  operator transforms as a (10)  $SU(3)$  tensor when  $\Delta\hbar\omega = +1$  in the transition and as a (01)  $SU(3)$  tensor when  $\Delta\hbar\omega = -1$ . Thus in the  $1_1^- \rightarrow 0_1^+$  transition in  $^{14}\text{C}$  the (23) and (31) components of the  $1_1^-$  wave function (86.7%) do not contribute and in the  $0_2^+ \rightarrow 1_1^-$  transition the first six  $SU(3)$  configurations in the  $0_2^+$  wave functions (90.5%) do not contribute. The  $B(E1; 0_2^+ \rightarrow 1_1^-)$  calculated from the wave functions of Table IV gives a lifetime for the  $0_2^+$  level which, within errors, is in agreement with the present measurement. This  $B(E1)$  is sensitive to changes in the  $1s_{1/2}$  single-particle energy; a lowering of the  $1s_{1/2}$  level by 0.5 MeV increases

the  $B(E1)$  from  $3.3 \times 10^{-3}$  Weisskopf units (W.u.) to  $5.7 \times 10^{-3}$  W.u. The  $B(E1; 1_1^- \rightarrow 0_1^+)$  is considerably larger, and is stable with respect to variations of the single-particle energies, leading to a predicted 0.4-fs lifetime for the  $1_1^-$  level. Since the  $E1$  matrix element for  $0_1^+ \rightarrow 1_1^-$  is larger than that for  $0_2^+ \rightarrow 1_1^-$ , a small destructive admixture of  $0_1^+$  into  $0_2^+$  can change significantly the predicted lifetime of the  $0_2^+$  level. When  $0\hbar\omega - 2\hbar\omega$  mixing is included in the calculation described above,  $B(E1; 0_2^+ \rightarrow 1_1^-)$  decreases by almost an order of magnitude (see Table III), spoiling the good agreement with the measured matrix element. However, there are difficulties, which are elaborated upon below, in

TABLE IV. SU(3) intensities for  $A = 14$  wave functions.

$J_n^\pi$	$T$	(02)	(10)							
$0_1^+$	1	71.64	28.36							
$1_1^+$	0	92.13	7.87							
$1_2^+$	0	92.17	7.83							
		(44)	(06)	(14)	(25)	(52)	(60)	(33)	(22)	(41)
$0_2^+$	1	66.37	6.84	0.74	4.89	9.30	2.29	5.11	3.04	1.41
$1_3^+$	0	69.77	6.24	0.66	1.43	10.37	2.30	5.05	2.80	1.37
		(23)	(31)	(12)	(20)	(01)				
$0_1^-$	1	56.02	21.47	12.10	3.11	7.30				
$1_1^-$	1	65.95	20.74	6.68	1.68	4.97				
$2_1^-$	1	77.34	11.13	9.03	1.96	0.55				
$3_1^-$	1	59.22	27.16	11.32	2.29	0.00				
$0_1^-$	0	52.33	27.52	11.10	3.93	5.22				
$1_1^-$	0	52.48	29.45	9.53	3.33	5.21				
$2_1^-$	0	46.76	20.99	19.54	9.60	3.12				
$3_1^-$	0	51.12	34.27	10.53	4.07	0.01				
$4_1^-$	0	74.08	11.86	13.77	0.30	0.00				

performing a consistent calculation when  $\Delta\hbar\omega = 2, 4, \dots$  mixing is permitted.

In the case of no  $0\hbar\omega$ - $2\hbar\omega$  mixing the binding energies of the  $^{14}\text{C}$  levels are approximately correct when single-particle energies appropriate to an  $^{16}\text{O}$  core are used. Indeed, the calculated excitation energies of the  $1_1^-$ ,  $0_2^+$ ,  $3_1^-$ ,  $0_1^-$ , and  $2_1^-$  states are 6.12, 6.59, 6.52, 7.60, and 7.44 MeV, respectively. When mixing is allowed the binding energy of the  $0_2^+$  level decreases by only 230 keV while that of the ground state increases by 5.6 MeV. Similarly for the  $1^+, 0$  levels the binding energy of  $1_3^+$  decreases by 180 keV while the binding energies of  $1_1^+$  and  $1_2^+$  increase by 4.7 and 6.9 MeV, respectively. The depression of the  $0\hbar\omega$  states is caused by mixing with states of the (22) configuration which occur at relatively high excitation energies (20–30 MeV). This mixing occurs through the

dominant tensor in the  $\Delta\hbar\omega = 2$  central interaction which transforms as (20) under SU(3). The (42) tensor which mixes the dominant (02) and (44) components of the  $0_1^+$  and  $0_2^+$  wave functions is much weaker. Table V, which gives some details of the mixing, shows that most of the 15–20%  $2\hbar\omega$  admixture into the  $0\hbar\omega$  levels is accounted for by (22) configurations. If the  $4\hbar\omega$  configuration which could couple to the dominant (44) configuration of the  $0_2^+$  level via a (20) tensor were included the  $0_2^+$  level would be pushed down perhaps restoring to a large degree the original  $0_1^+ \sim 0_2^+$  separation of the no-mixing calculation. Clearly the binding energies of the lowest  $0^+$  levels will converge slowly as a function of  $N$ , where  $N\hbar\omega$  is the unperturbed energy of the most highly excited configuration included in the basis. Such a situation is familiar from extended shell-model calculations<sup>27, 28</sup> and from related cluster-model calculations using the orthogonality condition model (e.g., Ref. 29). Naturally, the negative-parity basis should be extended in a similar manner even though the lowest  $3\hbar\omega$  configurations occur at quite high excitation energies. In general, the  $\Delta\hbar\omega = 2$  admixtures lead to strong enhancements of certain in-band  $E2$  transitions which is desirable [the  $E2$  operator for  $|\Delta\hbar\omega| = 2$  transforms as (20)+(02)]. However, since  $E1$  matrix elements between low-lying levels involve much cancellation, a reliable calculation is much more difficult and systematic surveys

TABLE V.  $0\hbar\omega$ - $2\hbar\omega$  admixtures.

$J_n^\pi$	% $0\hbar\omega$	% $2\hbar\omega$	% 2p-2h	% 1p-1h	% (22)
$0_1^+$	82.76	17.24	12.66	4.58	13.87
$1_1^+$	85.22	14.78	12.22	2.55	11.10
$1_2^+$	79.06	20.94	16.76	4.18	16.13
$0_2^+$	1.65	98.35	97.77	0.57	2.64
$1_3^+$	1.16	98.84	98.03	0.80	3.06



will be required to demonstrate whether the use of extended shell-model spaces can lead to better estimates of  $E1$  matrix elements. It should be noted that the truncation scheme employed in Lie's weak-coupling calculation largely eliminates the (22) configurations from the  $2\hbar\omega$  basis with the result that the  $2\hbar\omega$  admixtures in the  $^{14}\text{N}$  and  $^{14}\text{C}$  ground states are not large. For similar reasons the  $3\hbar\omega$  components in the lowest negative-parity levels are very small. For many purposes such a truncation of the basis may be preferable to using the extended shell-model basis in which it is difficult to include consistently enough of the highly excited configurations to approach any sort of convergence in the calculation. However, since the  $E1$  operator can connect some of the strongly admixed (22) configurations to the dominant (23) and (31) configurations of the negative-parity wave functions, it is of interest to study the effect on transition rates of these  $2\hbar\omega$  admixtures in the  $0_1^+$ ,  $1_1^+$ , and  $1_2^+$  wave functions. Accordingly, in Table III we list electromagnetic matrix elements for both the no-mixing and mixing (bracketed numbers) cases. We use bare  $g$  factors and charges for all multipolarities except  $E2$  in which case we use an isoscalar effective charge which is double the bare value. The number of matrix elements listed goes well beyond those directly relevant to the lifetimes whose measurement is described in this paper. Included are  $E1$  and  $M2$  matrix elements not calculated by Lie; matrix elements involved in the decays of the  $2^-$  levels which are the partners, in weak-coupling doublets, of the  $3^-$  levels investigated in this paper; matrix elements for other  $\Delta\pi = -1$  decays which involve the lowest  $0^+$  and  $1^+$  levels; and matrix elements for transitions between negative-parity levels included for completeness or because new experimental information has become available since the work of Lie. Matrix elements for isospin forbidden transitions are not included. Finally, Table III contains an up to date collection of the available experimental data on these matrix elements. For each multipolarity we briefly discuss the agreement between theory and experiment.

Comparison is possible for three  $E3$  matrix elements. We note that for the transitions in  $^{14}\text{N}$  there is excellent agreement between the  $B(E3)$  values derived from the lifetimes and mixing ratios and those obtained from inelastic electron scattering.<sup>24</sup>

The  $B(E3)$  for the  $^{14}\text{N}$  5.11-0 transition in the no-mixing case agrees with experiment while the  $B(E3)$  for the  $^{14}\text{N}$  5.83-0 transition is a factor of 2 too low; in the range  $q = 0.7-1.2 \text{ fm}^{-1}$  investigated in Ref. 24,  $C3$  form factors calculated from our wave functions agree well with the data for the

$^{14}\text{N}$  5.11-MeV transition and are 40% too low for the  $^{14}\text{N}$  5.83-MeV transition. It is interesting that the inclusion of  $2\hbar\omega$  admixtures has little effect on the  $B(E3)$  for the 5.11-MeV state while giving a substantial enhancement to the  $B(E3)$  for the  $^{14}\text{N}$  5.83-MeV state. For the  $^{14}\text{C}$  6.73-0 transition there is naturally a cancellation between the isoscalar and isovector contributions to the  $E3$  matrix element which is therefore a sensitive function of any effective charge used; for the no-mixing case an isoscalar effective charge of  $0.79e$  (the bare value is  $0.5e$ ) reproduces the experimental  $B(E3)$  value. Again the  $B(E3)$  is enhanced by the inclusion of  $2\hbar\omega$  admixtures in the ground-state wave function. An even more substantial enhancement is expected from the inclusion of  $3\hbar\omega$  admixtures in the negative-parity wave functions. It is worth noting that the use of effective charges of  $1.5e$  for protons and  $0.5e$  for neutrons, such as are necessary to reproduce in a similar calculation the  $B(E3)$  values in the neighboring  $4n$  nuclei  $^{12}\text{C}$  and  $^{16}\text{O}$ , would give  $B(E3)$  values in  $A = 14$  which are too large by a factor of 2 to 3. This is perhaps a reflection of the simple weak-coupling structure of the low-lying negative-parity states in  $A = 14$ .

Of the five  $M2$  matrix elements four are in reasonable agreement with experiment and the remaining one, for the  $^{14}\text{N}$  5.11-0 transition, is extremely sensitive with respect to  $2\hbar\omega$  admixtures. The  $E1$  matrix elements are also rather sensitive to  $2\hbar\omega$  admixtures. In most of the eight cases one or another of the theoretical  $B(E1)$  values is within a factor or 2 of experiment. We regard this as reasonable agreement for these hindered transitions; the largest  $B(E1)$ —for  $^{14}\text{N}$  8.79-0—is actually in quite close agreement with experiment. For the  $M1$  transitions there is good agreement between theory and experiment for the stronger transitions but the agreement is often not so good for the weaker ones such as  $^{14}\text{C}$  7.34-6.09 and 7.34-6.73 and  $^{14}\text{N}$  8.91-5.11.

There are only two measured  $E2$  matrix elements. The agreement between theory and experiment is moderately good when the usual effective charges of  $1.5e$  and  $0.5e$  for protons and neutrons are used. Finally, for the six measured dipole-quadrupole mixing ratios the predicted signs are all in agreement with the measurement.

#### IV. CONCLUSIONS

The primary experimental result presented in this paper is the lifetime of the 6590-keV level in  $^{14}\text{C}$ . In the case of no  $0\hbar\omega-2\hbar\omega$  mixing, the shell-model calculation gives a lifetime in good agreement with the measured one. However, the  $E1$

matrix element involved is sensitive to configuration mixing and to the  $sd$ -shell single particle energies (and hence to the particle-hole interaction). Some aspects of the  $0\hbar\omega$ - $2\hbar\omega$  mixing have been discussed and the inconsistencies inherent in such a calculation have been pointed out. A next step would be to include at least  $4\hbar\omega$  configurations in the basis and at the same time to restrict the basis for  $2\hbar\omega$ ,  $4\hbar\omega$ , ... to those configurations which are strongly mixed by the dominant central component of the effective interaction. While the sizes of the matrices involved in such a calculation may not be prohibitively large, it is beyond the scope of existing shell-model codes to calculate all the required matrix elements. A measure-

ment of the radiative width of the 6.09-MeV  $1^-$  level of  $^{14}\text{C}$  would provide a very good test of the present calculations.

#### ACKNOWLEDGMENTS

D. Fields of Tennessee Technological University (TTU) performed the calculations of plunger capacitance and assisted in taking the experimental data. The hospitality, assistance, and cooperation of the BNL Tandem Laboratory staff are gratefully appreciated by the visitors from TTU. This research was supported by the Department of Energy.

- 
- <sup>1</sup>I. Unna and I. Talmi, *Phys. Rev.* **112**, 452 (1958).  
<sup>2</sup>E. K. Warburton, H. J. Rose, and E. N. Hatch, *Phys. Rev.* **114**, 214 (1959).  
<sup>3</sup>E. K. Warburton and W. T. Pinkston, *Phys. Rev.* **118**, 733 (1960).  
<sup>4</sup>F. Ajzenberg-Selove, *Nucl. Phys.* **A268**, 1 (1976); **A281**, 1 (1977).  
<sup>5</sup>H. Grawe, J. Herholz, and K. Kandler, *Z. Phys. A* **276**, 351 (1976).  
<sup>6</sup>D. E. Alburger and E. K. Warburton, *Phys. Rev.* **132**, 790 (1963); E. K. Warburton, D. E. Alburger, A. Gallmann, P. Wagner, and L. F. Chase, Jr., *ibid.* **133**, B42 (1964).  
<sup>7</sup>D. E. Alburger, A. Gallmann, J. B. Nelson, J. T. Sample, and E. K. Warburton, *Phys. Rev.* **148**, 1050 (1966).  
<sup>8</sup>D. B. Fossan and E. K. Warburton, in *Nuclear Spectroscopy and Reactions*, Part C, edited by J. Cerny (Academic, New York, 1974), p. 307.  
<sup>9</sup>T. K. Alexander and A. L. Bell, *Nucl. Instrum. Methods* **81**, 22 (1970).  
<sup>10</sup>K. W. Jones, A. Z. Schwarzschild, E. K. Warburton, and D. B. Fossan, *Phys. Rev.* **178**, 1773 (1969).  
<sup>11</sup>R. L. Kozub, J. Lin, J. F. Mateja, C. J. Lister, and E. K. Warburton, *Bull. Am. Phys. Soc.* **24**, 817 (1979).  
<sup>12</sup>M. Toulemonde, K. H. Souw, J. C. Adloff, and N. Schultz, *Phys. Rev. C* **22**, 553 (1980).  
<sup>13</sup>K. W. Allen, T. K. Alexander, and D. C. Healey, *Can. J. Phys.* **46**, 1575 (1968).  
<sup>14</sup>T. J. Moorhouse, J. Asher, D. W. Bennett, H. A. Doubt, M. A. Grace, P. D. Johnson, W. L. Randolph, and P. M. Rowe, *J. Phys. G* **4**, 1593 (1978).  
<sup>15</sup>K. W. Allen, T. K. Alexander, and D. C. Healey, *Phys. Lett.* **22**, 193 (1966).  
<sup>16</sup>R. A. I. Bell, R. D. Gill, B. C. Robertson, J. S. Lopes, and H. J. Rose, *Nucl. Phys.* **A118**, 481 (1968).  
<sup>17</sup>R. S. Blake, D. J. Jacobs, J. O. Newton, and J. P. Shapira, *Phys. Lett.* **14**, 219 (1965); S. Gorodetzky, R. M. Freeman, A. Gallmann, and F. Haas, *Phys. Rev.* **149**, 801 (1966).  
<sup>18</sup>H. J. Rose and D. M. Brink, *Rev. Mod. Phys.* **39**, 306 (1967).  
<sup>19</sup>S. Lie, *Nucl. Phys.* **A181**, 517 (1972).  
<sup>20</sup>D. J. Millener and D. Kurath, *Nucl. Phys.* **A255**, 315 (1975).  
<sup>21</sup>S. Cohen and D. Kurath, *Nucl. Phys.* **73**, 1 (1965).  
<sup>22</sup>W. Chung, Ph.D. thesis, Michigan State University, 1976 (unpublished).  
<sup>23</sup>S. J. Skorka, J. Hertel, and T. W. Retz-Schmidt, *Nucl. Data, Sect. A* **2**, 347 (1966).  
<sup>24</sup>N. Ensslin, W. Bertozzi, S. Kowalski, C. P. Sargent, W. Turchinets, C. F. Williamson, S. O. Fivozinsky, J. W. Lightbody, and S. Penner, *Phys. Rev. C* **9**, 1705 (1974).  
<sup>25</sup>A. Gallmann, F. Haas, and B. Heusch, in *Contributions to the International Conference on Properties of Nuclear States, Montreal, 1969*, edited by M. Harvey *et al.* (Presses de l'Université de Montréal, Montréal, Canada, 1969), pp. 116 and 692.  
<sup>26</sup>J. Keinonen, A. Anttila, and M. Bister, *Nucl. Phys.* **A294**, 1 (1978).  
<sup>27</sup>T. Tomoda and A. Arima, *Nucl. Phys.* **A303**, 217 (1978).  
<sup>28</sup>F. Arickx, J. Broeckhove, and E. Deumens, *Nucl. Phys.* **A318**, 269 (1979).  
<sup>29</sup>Y. Suzuki, *Prog. Theor. Phys.* **55**, 1751 (1976); **56**, 111 (1976).